

Open-radiomics: A Research Protocol to Make Radiomics-based Machine Learning Pipelines Reproducible

Ernest (Khashayar) Namdar^{1,5,6}, Matthias W. Wagner^{2,5}, Birgit B. Ertl-Wagner^{2,5}, Farzad Khalvati^{1,2,3,4,5,6}

1. Institute of Medical Science, University of Toronto, Toronto, ON, Canada
2. Department of Medical Imaging, University of Toronto, Toronto, ON, Canada
3. Department of Computer Science, University of Toronto, Toronto, ON, Canada
4. Department of Mechanical and Industrial Engineering, University of Toronto, Toronto, ON, Canada
5. Department of Diagnostic Imaging, Neurosciences & Mental Health Research Program, The Hospital for Sick Children (SickKids), Toronto, ON, Canada
6. Vector Institute, Toronto, ON, Canada

Abstract. The application of artificial intelligence (AI) techniques to medical imaging data has yielded promising results. As an important branch of AI pipelines in medical imaging, radiomics faces two major challenges namely reproducibility and accessibility. In this work, we introduce open-radiomics, a set of radiomics datasets, and a comprehensive radiomics pipeline that investigates the effects of radiomics feature extraction settings such as binWidth and image normalization on the reproducibility of the radiomics results performance. To make radiomics research more accessible and reproducible, we provide guidelines for building machine learning (ML) models on radiomics data, introduce Open-radiomics, an evolving collection of open-source radiomics datasets, and publish baseline models for the datasets.

Keywords: radiomics, open-source, dataset, tabular, reproducibility

Introduction

Artificial Intelligence (AI) has found its applications across different fields, and medical imaging is one of the high potential contexts where AI solutions are promising [1]–[3]. Machine Learning (ML) is a subset of AI with tools for classification, regression, and decision making, with many applications for medical imaging data [4]. ML algorithms in medical imaging fulfill tasks such as Region of Interest (ROI) segmentation and classification, and they are used as building blocks of AI-based pipelines for diagnosis, prognosis, and therapeutic assessments.

Deep Learning (DL) is a branch of ML where multiple-layer Neural Networks (NN) are utilized at its core. Currently, AI-based segmentation is usually conducted using DL algorithms. However, in the realm of ML-based classification of medical imaging data, DL has a well-established competitor called radiomics. The suffix “omics” refers to a large set of manually-defined features, and it manifests across different domains such as radiomics in Radiology, and genomics in Genetics. From the Data Science point of view, radiomics provides mapping i.e., converting images into tabular data. Usually, radiomics studies start with image annotation where 2D/3D Regions of Interest (ROIs) are segmented. Each radiomics feature is the result of applying a distinct equation to the ROI. Once the radiomics features are extracted, any ML classifier capable of handling tabular data, such as Random Forests (RF), can be used to perform the classification task. Fig. 1 illustrates a typical radiomics-based classification/regression pipeline.

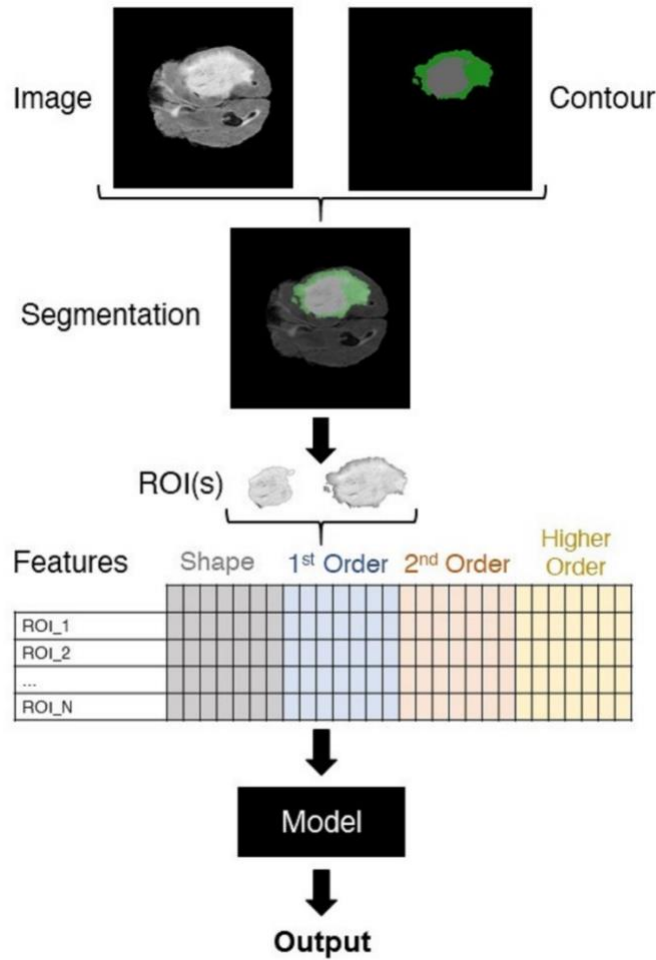


Figure 1. Overview of a radiomics-based classification pipeline [4]

In comparison to DL, radiomics offers a higher degree of explainability since its features are derived using transparent equations. However, there are multiple sources of variability impacting their generalizability and reproducibility [5]. Radiomics features are sensitive to any form of change in ROIs (i.e., if intensity values of image pixels/voxels within an ROI are manipulated). Different vendors, imaging device settings, imaging protocols, contouring discrepancy (known as intra- and inter-reader variability), image normalization, and radiomics extraction settings might result in variation in radiomics results. Insufficient technical details such as data split information, and lack of openness to the data and codes are other obstacles to having reproducible radiomics research. Depending on the source of the variability, addressing the issue might be infeasible in a given study. An example is tackling intra- and inter-reader variability in a fixed dataset of radiology images and ROI segmentations without further information about the reader, similar to the dataset of the current study. Nevertheless, all these sources of variability create a demand for a proper statistical approach for measuring the randomness of radiomics studies. Unfortunately, radiomics studies often lack systematic randomness measurements. Hence, in this research, we aim to provide an open-source radiomics dataset along with a baseline classification pipeline. We propose a robust protocol for radiomics pipelines, targeting reproducible radiomics-based classification models.

In this research, we use the BraTS 2020 [10][11][12], an open-source multimodal Magnetic Resonance Imaging (MRI) dataset for brain tumor segmentation. Because BraTS is primarily a segmentation dataset, the majority of articles in the literature are dedicated to contouring brain tumors [10], [12], [15]. P.Dequidt et al. [14] used BraTS 2018 to conduct their radiomics-based HGG/LGG classification. Five expert radiologists labeled the tumors based on WHO standards, which enabled them to compare their model against another set of ground truths in addition to the BraTS

labels. They extracted a limited set of radiomics (51 features for each MRI sequence), used Support Vector Machines (SVM)[16] as their classifier with a 5-fold cross-validation for hyperparameter optimization, and achieved 84.1% accuracy with reference to the BraTS ground truths. M. Coupet et al. [17] use BraTS 2020 as one of the datasets to train their models. Nonetheless, they form a healthy/glioma classification framework. F. P. Polly et al., apply Otsu thresholding [18] to the images, use k-means for segmentation, Discrete Wavelet Transform (DWT) for feature extraction, Principal Component Analysis (PCA) for dimensionality reduction, followed by SVM for a two-stage classification: abnormal/normal and then HGG/LGG. They achieve 99% accuracy on a small and balanced subset (50 HGG and 50 LGG) of BraTS 2017 and BraTS 2013 datasets, with a one-time data split approach.

Given the chosen dataset, we investigate the effect of image normalization, the most crucial radiomics feature extraction hyperparameter, imaging sequence, and tumor subregion on a radiomics-based tumor type classification pipeline.

Material and Methods

While there is annotated open-source medical imaging data, the extracted radiomics features are not usually available. Thus, each researcher must decide the appropriate tools/libraries and settings to extract the features. Consequently, radiomics studies are often conducted on small internal datasets with a narrowed-down selection of hyperparameters for extracting the features. Open-radiomics¹ is our initiative for open-source large-scale radiomics datasets where we provide AI-ready tabular datasets along with baselines.

One of the sources of variability in the radiomics research is the discrepancy between the feature extraction software and packages used across the studies. Multiple options are available to the research community for radiomics feature extraction [6], [7]. Nonetheless, their back-ends might be dissimilar, leading to irreproducibility of radiomics research. We will use PyRadiomics[8], which is widely used and supported by a large and established community. It should be highlighted that PyRadiomics based packages such as the Slicer Radiomics add-on module for 3D Slicer² software[9] might mask some features of PyRadiomics, resulting in suboptimal feature extraction.

Dataset

The dataset is a collection of multisequence MRIs including T1-weighted (T1), gadolinium based contrast agent (GBCA) enhanced T1-weighted (T1CE), T2-weighted (T2), and T2 Fluid-Attenuated Inversion Recovery (FLAIR) sequences. The training cohort of BraTS 2020 is the data applicable to our research because its ground truth (GT) ROI segmentations are available. The cohort includes 369 adult patients with brain tumors, of which 76 cases are low-grade glioma (LGG), and 293 are high-grade glioma (HGG) tumors. The images are all co-registered to the SRI24 atlas[13], skull stripped, resampled to 1 mm³, and their size is unified to 155 × 240 × 240. We acknowledge that there is a discrepancy in the definition of LGG and HGG between BraTS and the World Health Organization (WHO) [14]. In this paper, we follow the binary grading system (HGG vs. LGG) provided by BraTS.

BraTS 2012-2016 included four tumor subregions, labeled 1-4. The necrotic (NCR), and the non-enhancing (NET) tumor core were labeled 1 and 3, respectively. Label 2 corresponded to the peritumoral edematous/invaded tissue (ED), and active tumor (AT) was labeled 4. Since BraTS 2017, NET and NCR are combined, and label 3 is removed from the annotations. Fig. 2 depicts one slice of an image volume along with its corresponding segmentation mask. We analyze the whole tumor (all four subregions), AT, ED, and the union of NCR and NET (NETnNCR), in separate scenarios. In Fig. 2., the orange area is AT, the green area is ED, and the gray parts are NETnNCR.

¹ <https://openradiomics.org>

² <https://www.slicer.org/>

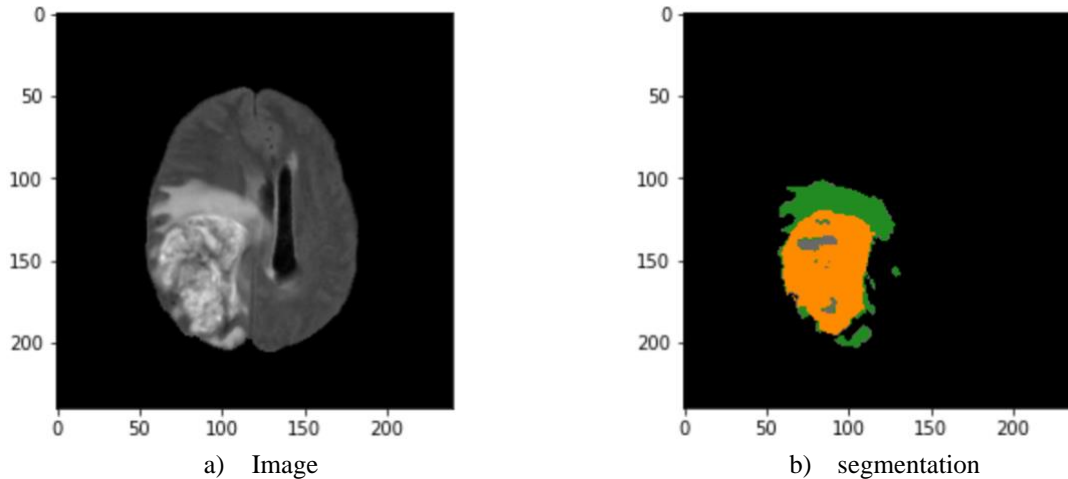


Figure 2. An example image (the FLAIR sequence) and its corresponding segmentation mask

Data preparation

We utilized the PyRadiomics library to extract radiomics features of ROIs from images normalized with different techniques. RF was selected as the classification algorithm, and a repeated data splitting approach was implemented to provide a context for measuring randomness.

PyRadiomics Library

Radiomics feature extraction using PyRadiomics is a sophisticated task, and there are several technical points to be considered. Installation of the trimesh python package is crucial for radiomic feature extraction³ to ensure calculation of all feature categories. Although no randomness is involved in the feature extraction process, seeding is recommended in all the codes. This improves reproducibility of the results if random IDs are assigned to ROIs, or further analysis such as dimensionality reduction and data visualization are incorporated into the scripts. We encourage extracting the full set of radiomics features, which is not enabled by default⁴.

In general, radiomics studies might be 2D or 3D. A 2D analysis is used when the imaging method is 2D, such as X-Ray. However, when 3D images are accessible, 2D and 3D radiomics analyses are possible. If the 2D approach is utilized with 3D images, often the analysis is done on the biggest tumor intersection. In the case of 3D analyses, such as this project, enabling the full set feature extraction forces the library to extract 2D Local Binary Pattern (LBP) features [19][20] in addition to the 3D LBP features. However, 2D shape features are skipped by PyRadiomics. In this condition, extra attention should be paid to the 2D features if they are not manually removed. From the Data Science point of view, 2D and 3D features are both valid for any scenario because there are distinct algorithms for extracting them. In this research we included 2D LBP features, and thus a full set of 1,710 features were extracted for each ROI.

PyRadiomics has multiple hyperparameters that affect the feature extraction procedure⁵. One of the most important is binWidth, which has been studied in the literature multiple times[21]. binWidth determines the bin size which is needed to form histograms used for discretizing gray levels in the image, and thus it affects all except shape features which are independent of pixel/voxel intensities. The default value of binWidth in PyRadiomics is 25. In this research,

³ Can be done through `pip install trimesh`

⁴ `extractor.enableAllImageTypes()` and `extractor.enableAllFeatures()` will result in a full set feature extraction

⁵ <https://pyradiomics.readthedocs.io/en/latest/customization.html>

in addition to 25, we examine 35 and 15 to see how they affect the results. All other hyperparameters are set to their default values.

Image normalization

Image normalization plays an important role in ML pipelines, which can influence radiomics significantly. We implemented histogram equalization [22], z-score [23], gamma [24], and minmax [25] image normalization methods and incorporated them into our 3D analyses. As the coefficients of our gamma normalization, we explored 0.5 and 1.5. The minmax normalization clips voxel values of the image volumes between 0 and 1. All the normalization methods were applied to the image volumes, not the ROIs. We did not investigate ROI normalization in this research because it would increase the computational load. Nonetheless, it can be studied in the future.

Data management

Data management is an essential part of radiomics studies. To avoid data fragmentation and possible mistakes, we suggest saving the features, GT labels, clinical variables, and any other information in a single csv file. Each row of the csv file (except the header row) should belong to a unique ROI. For the studies where a patient might have multiple ROIs, creating unique ROI IDs and appending them as the first column to the dataset is preferred. The naming of the radiomics datasets (csv files) is important. All names start with “Radiomics”, and the format is always csv. We use ‘_’ as the separator to include type of the normalization, and sequence in the naming. If needed, other pieces of information can be included. Obviously, no underscore should be used within the parts. Two examples of naming would be Radiomics_Gamma-0.5_FLAIR.csv, and Radiomics_NoNormalization_ED_T1.csv.

In this research, we study the effect of image normalization, imaging sequence, tumor subregion, and PyRadiomics settings on an adult brain tumor classification pipeline. As it was mentioned, we have 6 image normalization methods (i.e., NoNormalization, Gamma0.5, Gamma1.5, Histogram, ZScore, and MinMax), 4 imaging sequences (T1, T1CE, T2, FLAIR), 4 tumor subregions (i.e., whole tumor, AT, ED, and NETnNCR), 3 different binWidth values (i.e., 15, 25, and 35). This creates 288 sets of tabular datasets for the radiomic features (~2.9 GB of data).

Classification pipeline

Once feature extraction is completed, the classification modules can be designed and implemented. With the default settings of PyRadiomics, each dataset has a group of diagnostics features (e.g., python version, simple itk version, etc.), which will not contain differentiative information, and thus we filter them.

We employ a repetitive approach to measure randomness of our radiomics-based ML classification pipeline, which is illustrated in Fig. 3. We suggest the same approach be utilized in any radiomics study. We repeat our evaluations on the test sets N times⁶. In a for loop with N repetitions, in each iteration we randomly split our data into test (p%)⁷ and development (dev) sets. In the next step, a feature filtration algorithm is trained on the dev set and applied to the test set to randomly drop one of the features in pairs with a correlation coefficient above 0.95. Another layer of feature selection is Near-zero Variance (NZV) filtration. We train an algorithm on the dev set and apply it to the test cohort to remove any feature with a variance lower than 0.05. The last step of feature manipulation is a MinMax scaler which learns the transformations from the dev set and applies them to the test.

RF models are explainable and differentiative when applied to radiomics [26][27], and thus we chose them as our baseline classifiers. We defined a grid space for our classifier which is described in appendix A. For each combination of the hyperparameters in the grid space, we conduct N_{val} experiments⁸. In each experiment, the dev set is randomly split into training and validation (p_val%)⁹ cohorts. An instance of the classifier with the proposed hyperparameters is trained and evaluated based on the random split. While we use Area Under the Receiver Operating Characteristic Curve (AUROC) as our evaluation metric, any other criterion, such as accuracy, might be utilized. Nonetheless, all

⁶ 100 is the value of N which is used for this research

⁷ 20% for this project

⁸ In this research we had $N_{val} = 100$

⁹ 25% for this project

metrics are suitable for imbalanced datasets and medical contexts [28]. Once the N_{val} experiments are completed for the whole grid space, the best hyperparameter set is derived based on the highest average AUROC. To measure the validation performance, instances of models with the best hyperparameter set are trained and validated N_{val} times on random data splits with $p_{val}\%$ ratio. Average AUROC is considered to be the validation performance of the models. In the final step, an instance of the model with the best hyperparameters is trained on the entire dev set and evaluated on the test cohort. As it was mentioned, the whole process is repeated N times¹⁰, and thus we have N test AUROCs as well as N validations AUROC.

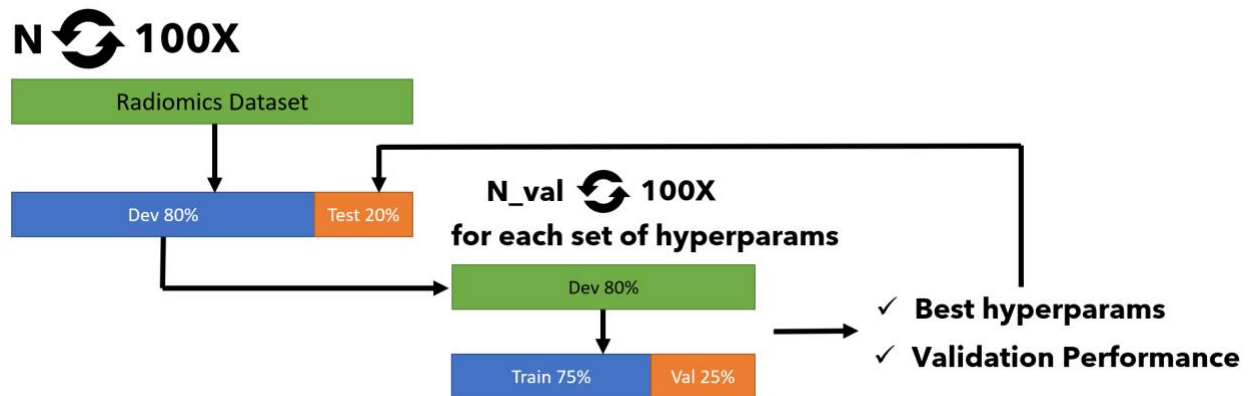


Figure 3. The repetitive classification approach

Other technical concerns

Radiomics-based ML pipelines are more explainable compared with DL, which is a result of the transparent definitions of the radiomic features. Radiomics studies usually are concluded by highlighting the most important features, and we encourage this approach. Not every algorithm is explainable. As an example, once an NN classifies a radiomics example, determining the influential features is perplexing. RF is an explainable model, and thus feature importances of an RF classifier can be derived. We capture the most important feature of each N experiments, for each dataset. Hence, we will have a list of $288 \times N$ top features, and the most frequent element of the list will represent the number one radiomics feature for BraTS 2020 tumor type classification. The last technical point is the choice of $N=100$ and $N_{val}=100$, which is made based on the practice of the Central Limit Theorem (CLT). This number of repetitions eliminates the need for k -fold cross-validation. Hence, we suggest setting N and N_{vals} above 30, where computational costs allow, and switching to k -fold cross-validation, otherwise.

Results

We investigated the effect of PyRadiomics binWidth, image normalization method, ROI subregion, and the MRI sequence on the radiomics-based ML brain tumor type classification pipeline. The results were structured to determine effects of the studied factors in terms of feature extraction failure and classification performance.

Feature Extraction Failure

Fig. 4-7 show impact of these factors on radiomics feature extraction failure. We define the failure as a fatal error or a timeout produced by the PyRadiomics library during the feature extraction. On a system with an AMD Ryzen threadripper pro 3955wx, 128 GB of RAM, 4 TB of M2 SSD, running Ubuntu 20.04.4 LTS, we set the timeout

¹⁰ In this research we had $N = 100$

threshold at 120 seconds which created a safe margin because common ROI feature extraction time was of the order of seconds.

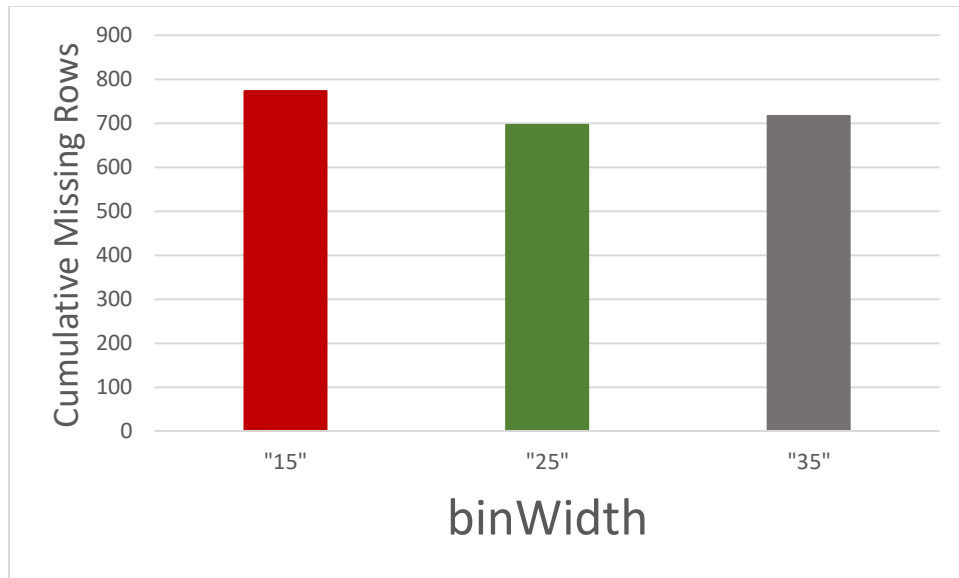


Figure 4. Effect of binWidth on failure of the radiomics feature extraction

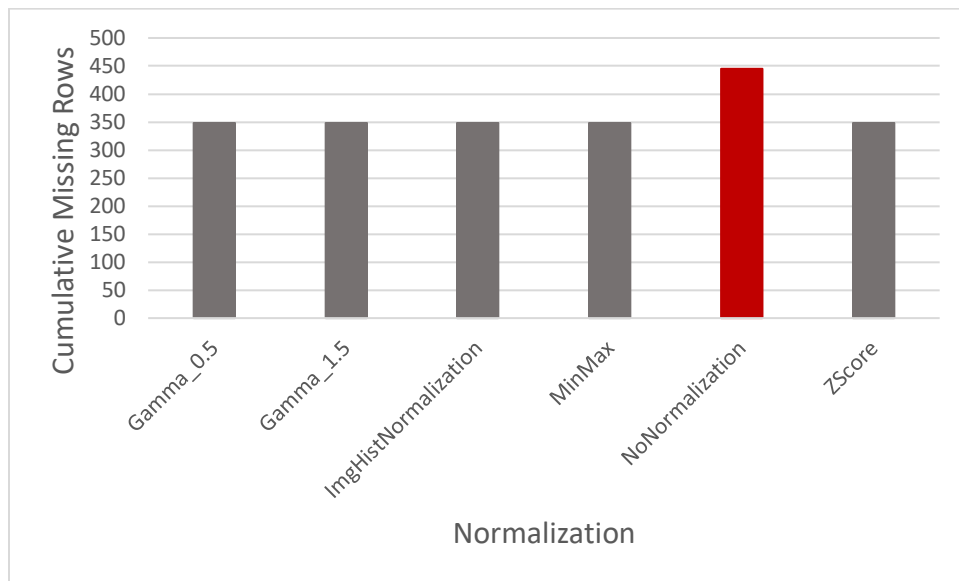


Figure 5. Effect of image normalization on failure of the radiomics feature extraction

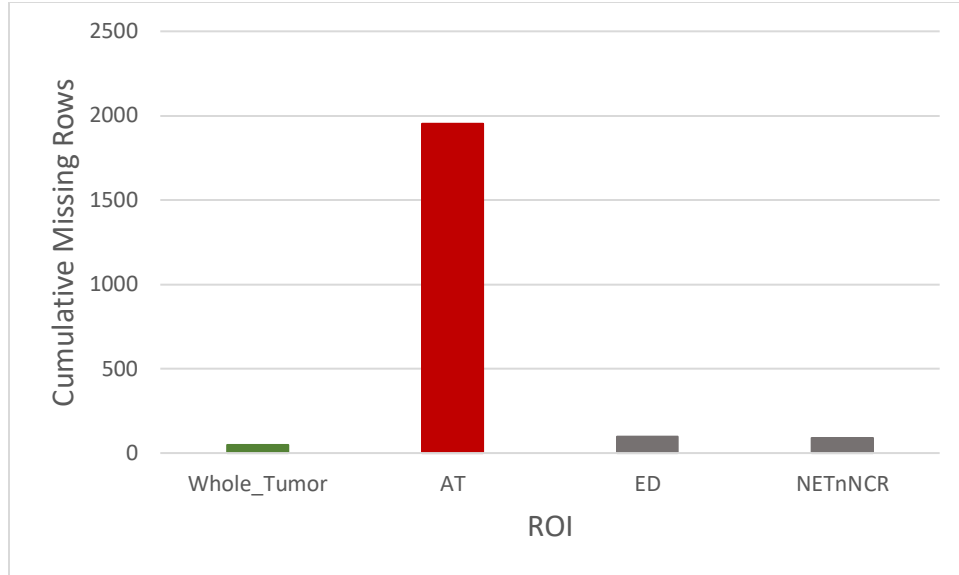


Figure 6. Effect of ROI on failure of the radiomics feature extraction

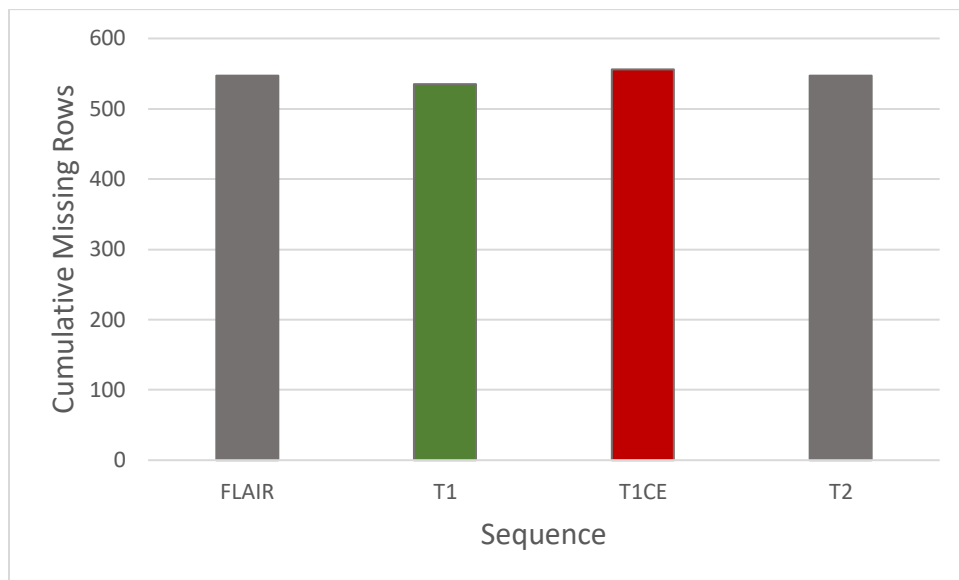


Figure 7. Effect of Sequence on failure of the radiomics feature extraction

Classification Performance

Fig. 8-11 illustrate the effect of the four sources of variability on the AUROC performance of the classifiers, for validation and test cohorts.

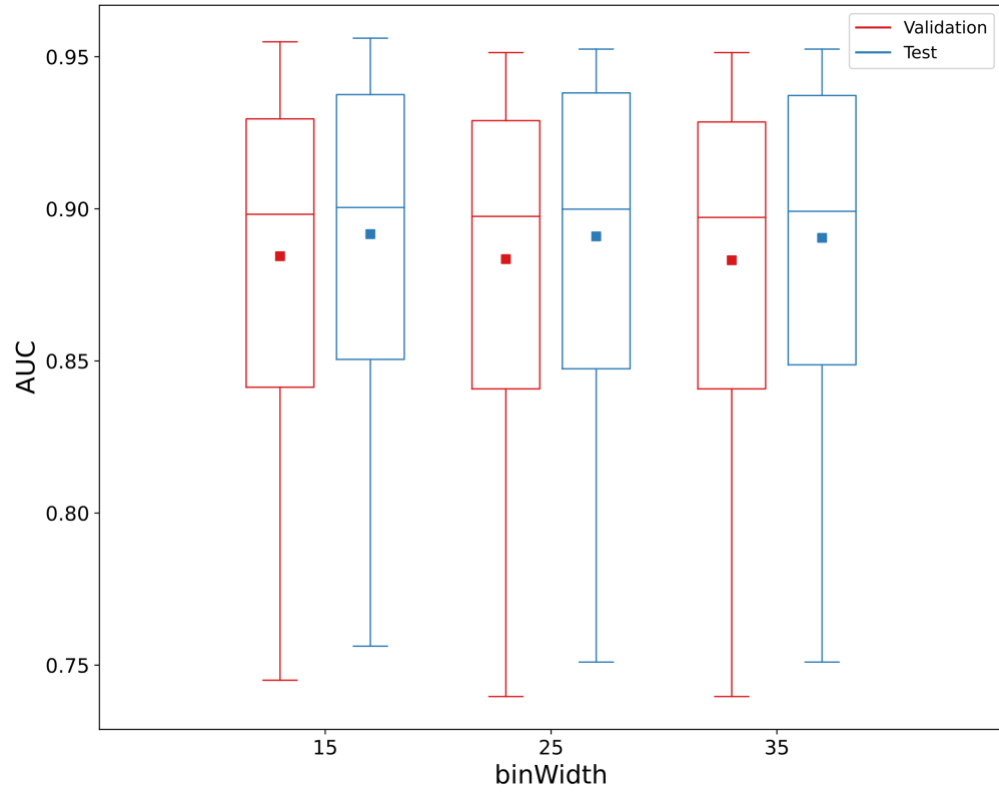


Figure 8. Effect of binWidth on AUROC performance of the classifiers

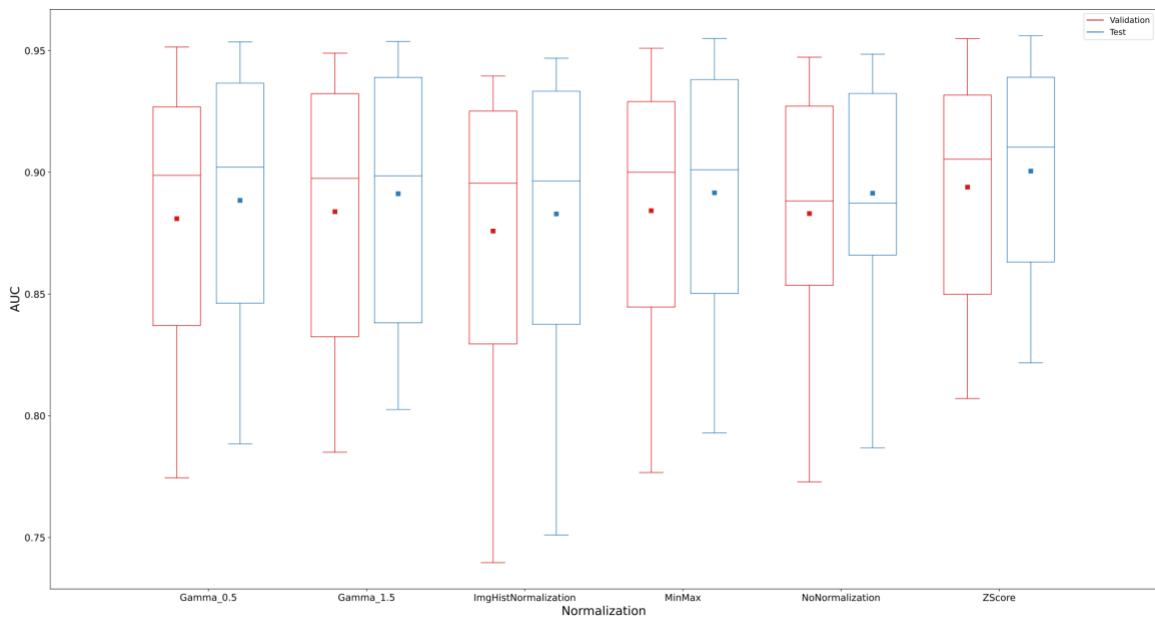


Figure 9. Effect of image normalization on AUROC performance of the classifiers

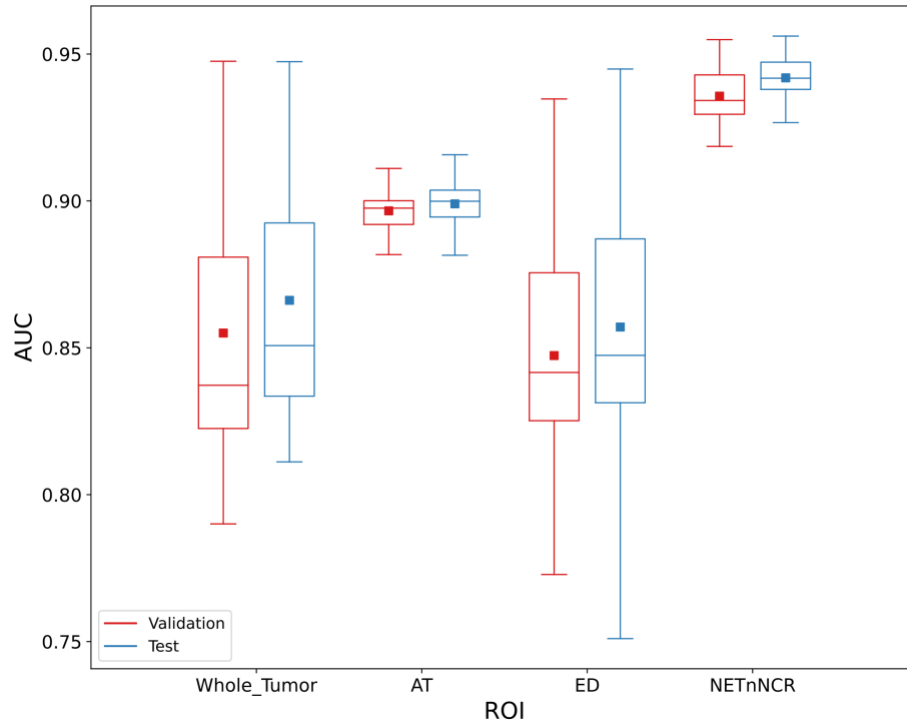


Figure 10. Effect of ROI subregion on AUROC performance of the classifiers

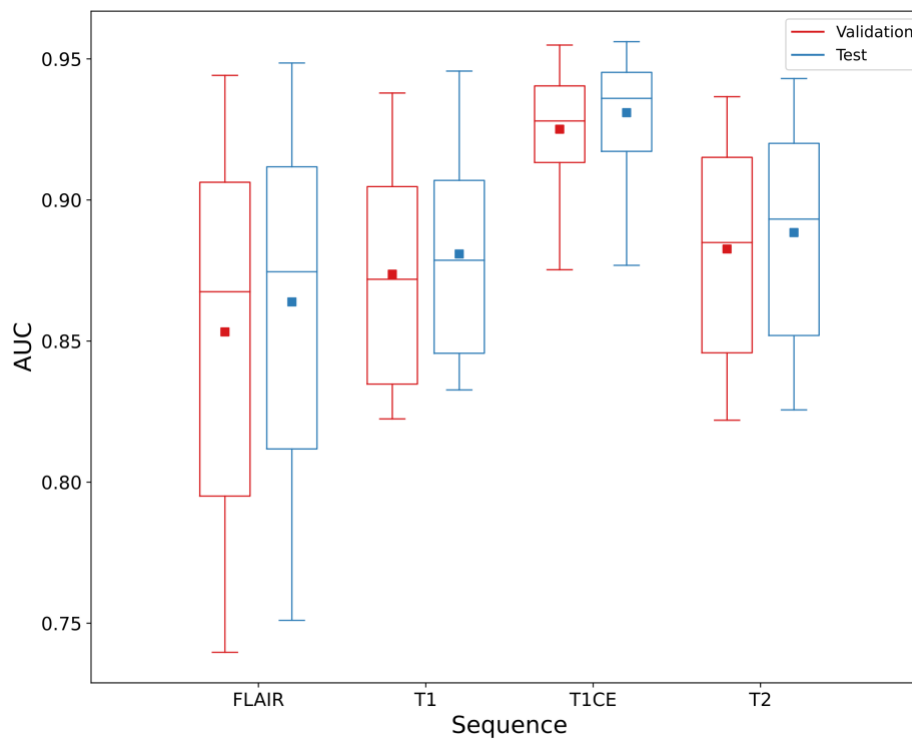


Figure 11. Effect of MRI sequence on AUROC performance of the classifiers

It should be highlighted the highest AUROC might not be achieved with the combination of the best image normalization, binWidth, tumor subregion, and MRI sequence. Our approach is repetition-based and can be considered as a stochastic or random process, whose output is individual AUROCs. We achieve the highest average AUROC performance across the 100 experiments on T1CE, for NETnNCR classification, with ZScore normalization, and with binWidth equal to 15, and its test AUROC was 0.956. The second and the third top performing datasets (mean test AUROCs equal to 0.955 and 0.954) had the same setting except for their image normalization, which was MinMax, and Gamma 1.5, respectively. Fig. 12 depicts how the top feature (`lbp-3D-k_glszm_HighGrayLevelZoneEmphasis`) differentiates the HGG and LGG examples on the top-performing dataset.

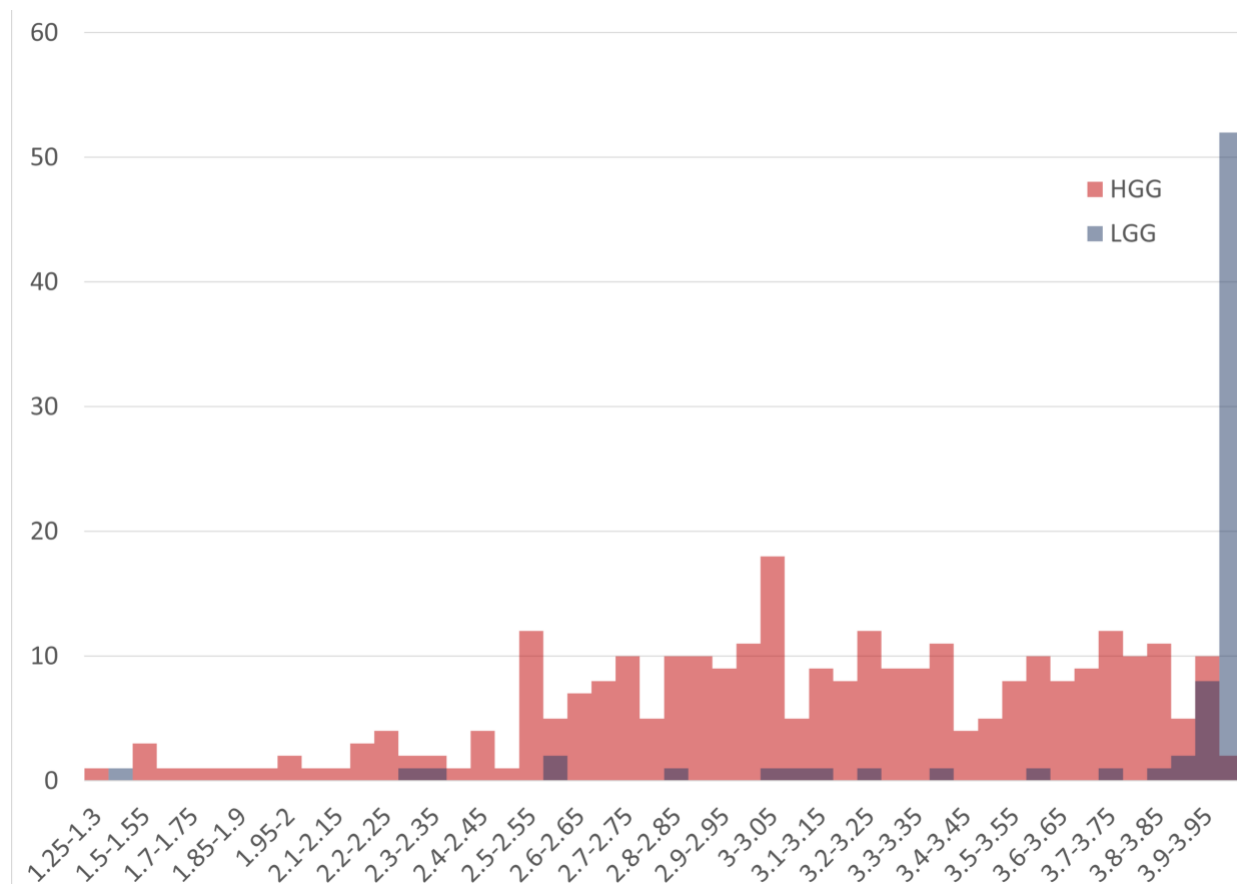


Figure 12. Histograms of the top feature on the top dataset: The horizontal axis represents bins of the feature values, and the vertical axis shows the number of ROIs with values in each bin.

It must be denoted that the boxplots in Fig 8-11 represent the range of average AUROCs. Hence, the maximum test performance of NETnNCR in Fig 10 is itself an average of 100 experiments. Thus, there are multiple experiments in which we achieve very high AUROCs. Obviously, such high results are not reproducible. Along with the mean for each dataset, we also captured min, median, max, and first and third quartile of the AUROC performances. In 140 datasets out of 288, the highest achievable AUROC was above 0.99. In 28 cases, including T1CE, ZScore normalization, whole tumor classification, binWidth15, we reached to AUROC of 1. Nonetheless, our results prove that AUROC of 1 for whole tumor classification is extremely irreproducible. Fig. 13 illustrates the range of AUROC performance of the top-ten datasets.

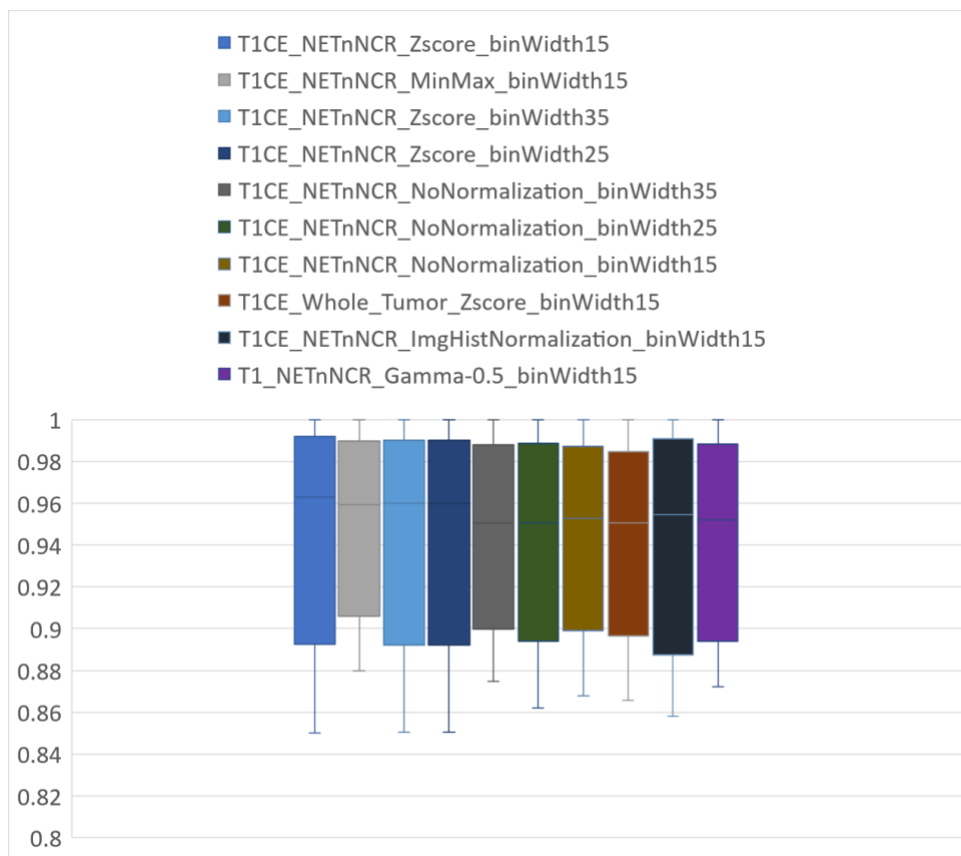


Figure 13. The 5 top-performing datasets

Discussion

It can be inferred that at least for the case of BraTS 2020, and from the number of missing cases point of view, the best PyRadiomics binWidth is 25, which is the default. While the type of image normalization does not make a significant difference, skipping normalization is suboptimal. The chance of having a successful feature extraction is increased if the subregion is bigger and more convex. Hence, the best case is whole tumor classification, and the worst case is AT. While the difference between the sequences is marginal, T1 and T1CE are the best and worst sequences, respectively.

Overall, binWidth does not make a tangible difference. Among the image normalization techniques we examined, ZScore slightly improved the average performance of the models. It also decreased the variance of the test AUROCs, which is another desirable point. Our results suggest the true potential of radiomics might not be exploited for whole tumor classification of BraTS 2020. In the case of ED, we observed the highest AUROC variances. In contrast, the models are surprisingly accurate and precise for NETnNCR classification of HGG and LGG tumors with an average test AUROC above 0.94. While for AT, the average test AUROCs lands below 0.90, the variance is low, and thus the results are reproducible. Among the four MRI sequences, T1CE surpasses the others significantly, and the lowest AUROC performances come out of FLAIR.

Except for the shape and first-order features, explaining the details and physical meaning of radiomics features is not straightforward. Radiomics includes multiple groups of features, which are described in the Image Biomarker Standardization Initiative (IBSI) [29]. LBPs are operators that label pixels (or voxels, in the case of 3D ROIs) of images based on thresholding their neighbor points [19]. To form the lbp-3D-k, PyRadiomics extracts the spherical kurtosis image using the `scipy.stats.kurtosis` function [30], and applies the LBP operator to it. Kurtosis is defined as the fourth central moment times inverse of the square of the variance, and the kurtosis image corresponds to calculating kurtosis for every voxel. In radiomics, Gray Level Size Zone (GLSZM) is used for quantifying gray level zones in

images. Gray level zones are defined as the number of connected voxels with similar gray level intensities. High Gray Level Zone Emphasis (HGLZE), which is formulated as Eq. 1, represents a measurement of the distribution of the higher gray-level values. Higher HGLZE means the ROI contains a greater proportion of higher gray-level values and size zones.

$$HGLZE = \frac{\sum_{i=1}^{N_g} \sum_{j=1}^{N_s} \frac{P(i,j)}{i^2}}{N_z} \quad \text{Eq. 1}$$

In Eq. 1., N_g and N_s correspond to the number of discrete intensity values, and the number of discrete zone sizes in the image, respectively. N_z is the number of zones in the ROI, and $P(i,j)$ is the size zone matrix.

Conclusion

In this research, we proposed a research protocol for radiomics-based ML pipelines to improve their reproducibility. We extracted and open-sourced a large series of tabular radiomics datasets based on the BraTS 2020 dataset that enables multiple opportunities for radiomics research. We established a reproducible baseline for the open radiomics datasets, and studied the effect of PyRadiomics binWidth, image normalization, ROI subregion, and the MRI sequence as four sources of variability of the results.

Our experiments demonstrated the default binWidth increases the chance of a successful ROI feature extraction, while it has no effect on the generalizability of the model. NETnNCR is associated with the highest performing models, and AT comes in second place. However, ED and whole tumor classifications will be challenging with radiomics features. We found T1CE and FLAIR to be the best and worst sequences, respectively.

The lbp-3D-k_glszm_HighGrayLevelZoneEmphasis radiomic feature appeared most frequently among the top features, and thus it is the most differentiative feature for HGG/LGG tumor type classification on BraTS 2020.

References

- [1] O. Ronneberger, P. Fischer, and T. Brox, "U-Net: Convolutional Networks for Biomedical Image Segmentation," pp. 1–8.
- [2] K. Namdar, I. Gujrathi, M. A. Haider, and F. Khalvati, "Evolution-based Fine-tuning of CNNs for Prostate Cancer Detection," *Int. Conf. Neural Inf. Syst.*, no. NeurIPS, 2019.
- [3] X. Liu *et al.*, "Can machine learning radiomics provide pre-operative differentiation of combined hepatocellular cholangiocarcinoma from hepatocellular carcinoma and cholangiocarcinoma to inform optimal treatment planning?," *Eur. Radiol.*, 2020, doi: 10.1007/s00330-020-07119-7.
- [4] M. W. Wagner, K. Namdar, A. Biswas, S. Monah, F. Khalvati, and B. B. Ertl-Wagner, "Radiomics, machine learning, and artificial intelligence—what the neuroradiologist needs to know," *Neuroradiology*, vol. 63, no. 12, pp. 1957–1967, 2021, doi: 10.1007/s00234-021-02813-9.
- [5] J. E. Park, S. Y. Park, H. J. Kim, and H. S. Kim, "Reproducibility and generalizability in radiomics modeling: Possible strategies in radiologic and statistical perspectives," *Korean J. Radiol.*, vol. 20, no. 7, pp. 1124–1137, 2019, doi: 10.3348/kjr.2018.0070.
- [6] L. Zhang, D. V. Fried, X. J. Fave, L. A. Hunter, J. Yang, and L. E. Court, "IBEX: an open infrastructure software platform to facilitate collaborative work in radiomics," *Med. Phys.*, vol. 42, no. 3, pp. 1341–1353, Mar. 2015, doi: 10.1118/1.4908210.

- [7] P. M. Szczypiński, M. Strzelecki, A. Materka, and A. Klepaczko, “MaZda--a software package for image texture analysis,” *Comput. Methods Programs Biomed.*, vol. 94, no. 1, pp. 66–76, Apr. 2009, doi: 10.1016/j.cmpb.2008.08.005.
- [8] J. J. M. van Griethuysen *et al.*, “Computational Radiomics System to Decode the Radiographic Phenotype,” *Cancer Res.*, vol. 77, no. 21, p. e104 LP-e107, Nov. 2017, doi: 10.1158/0008-5472.CAN-17-0339.
- [9] A. Fedorov *et al.*, “3D Slicer as an image computing platform for the Quantitative Imaging Network,” *Magn. Reson. Imaging*, vol. 30, no. 9, pp. 1323–1341, Nov. 2012, doi: 10.1016/j.mri.2012.05.001.
- [10] B. H. Menze *et al.*, “The Multimodal Brain Tumor Image Segmentation Benchmark (BRATS),” *IEEE Trans. Med. Imaging*, vol. 34, no. 10, pp. 1993–2024, Oct. 2015, doi: 10.1109/TMI.2014.2377694.
- [11] S. Bakas *et al.*, “Advancing The Cancer Genome Atlas glioma MRI collections with expert segmentation labels and radiomic features,” *Sci. data*, vol. 4, p. 170117, Sep. 2017, doi: 10.1038/sdata.2017.117.
- [12] S. Bakas *et al.*, “Identifying the Best Machine Learning Algorithms for Brain Tumor Segmentation, Progression Assessment, and Overall Survival Prediction in the BRATS Challenge.” 2018.
- [13] T. Rohlfing, N. M. Zahr, E. V Sullivan, and A. Pfefferbaum, “The SRI24 multichannel atlas of normal adult human brain structure,” *Hum. Brain Mapp.*, vol. 31, no. 5, pp. 798–819, May 2010, doi: 10.1002/hbm.20906.
- [14] P. Dequidt *et al.*, “Exploring Radiologic Criteria for Glioma Grade Classification on the BraTS Dataset,” *IRBM*, vol. 42, no. 6, pp. 407–414, 2021, doi: <https://doi.org/10.1016/j.irbm.2021.04.003>.
- [15] U. Baid *et al.*, “The RSNA-ASNR-MICCAI BraTS 2021 Benchmark on Brain Tumor Segmentation and Radiogenomic Classification.” 2021.
- [16] M. A. Hearst, S. T. Dumais, E. Osuna, J. Platt, and B. Scholkopf, “Support vector machines,” *IEEE Intell. Syst. their Appl.*, vol. 13, no. 4, pp. 18–28, 1998.
- [17] M. Coupet *et al.*, “A multi-sequences MRI deep framework study applied to glioma classification,” *Multimed. Tools Appl.*, 2022, doi: 10.1007/s11042-022-12316-1.
- [18] D. Liu and J. Yu, “Otsu Method and K-means,” in *2009 Ninth International Conference on Hybrid Intelligent Systems*, 2009, vol. 1, pp. 344–349, doi: 10.1109/HIS.2009.74.
- [19] T. Ojala, M. Pietikäinen, and T. Maenpää, “Multiresolution gray-scale and rotation invariant texture classification with local binary patterns,” *IEEE Trans. Pattern Anal. Mach. Intell.*, vol. 24, no. 7, pp. 971–987, 2002, doi: 10.1109/TPAMI.2002.1017623.
- [20] T. Ahonen, A. Hadid, and M. Pietikäinen, “Face Recognition with Local Binary Patterns BT - Computer Vision - ECCV 2004,” 2004, pp. 469–481.
- [21] M. Schwier *et al.*, “Repeatability of Multiparametric Prostate MRI Radiomics Features,” *Sci. Rep.*, vol. 9, no. 1, p. 9441, Jul. 2019, doi: 10.1038/s41598-019-45766-z.
- [22] X. Sun *et al.*, “Histogram-based normalization technique on human brain magnetic resonance images from different acquisitions,” *Biomed. Eng. Online*, vol. 14, no. 1, p. 73, 2015, doi: 10.1186/s12938-015-0064-y.
- [23] J. C. Reinhold, B. E. Dewey, A. Carass, and J. L. Prince, “Evaluating the Impact of Intensity Normalization on MR Image Synthesis,” *Proc. SPIE--the Int. Soc. Opt. Eng.*, vol. 10949, p. 109493H, Mar. 2019, doi: 10.1117/12.2513089.
- [24] S. Rahman, M. M. Rahman, M. Abdullah-Al-Wadud, G. D. Al-Quaderi, and M. Shoyaib, “An adaptive gamma correction for image enhancement,” *EURASIP J. Image Video Process.*, vol. 2016, no. 1, p. 35, 2016, doi: 10.1186/s13640-016-0138-1.
- [25] M. Kociolek, M. Strzelecki, and R. Obuchowicz, “Does image normalization and intensity resolution impact texture classification?,” *Comput. Med. Imaging Graph.*, vol. 81, p. 101716, 2020, doi:

<https://doi.org/10.1016/j.compmedimag.2020.101716>.

- [26] M. W. Wagner *et al.*, “Radiomics of pediatric low grade gliomas: toward a pretherapeutic differentiation of BRAF-mutated and BRAF-fused tumors,” *Am. J. Neuroradiol.*, 2021.
- [27] T. Ivanics *et al.*, “A pre-tace radiomics model to predict HCC progression and recurrence in liver transplantation. a pilot study on a novel biomarker,” *J. Transplant.*, 2020.
- [28] K. Namdar, M. A. Haider, and F. Khalvati, “A Modified AUC for Training Convolutional Neural Networks: Taking Confidence Into Account,” *Front. Artif. Intell.*, vol. 4, p. 155, 2021, doi: 10.3389/frai.2021.582928.
- [29] A. Zwanenburg *et al.*, “The Image Biomarker Standardization Initiative: Standardized Quantitative Radiomics for High-Throughput Image-based Phenotyping,” *Radiology*, vol. 295, no. 2, pp. 328–338, May 2020, doi: 10.1148/radiol.2020191145.
- [30] P. Virtanen *et al.*, “{SciPy} 1.0: Fundamental Algorithms for Scientific Computing in Python,” *Nat. Methods*, vol. 17, pp. 261–272, 2020, doi: 10.1038/s41592-019-0686-2.

Appendix A. Grid space of the RF models

Table 1. Grid space of the RF models

Hyperparameter	Grid Space
n_estimators	50, 100, 200
max_features	'auto', 'sqrt'
max_depth	None, 5, 10